Using Airborne LASER Altimetry and GIS to Assess Scale-Induced Radiation Loading Errors in a Glacierised Basin

LAURA CHASMER[1] AND CHRIS HOPKINSON[2]

ABSTRACT

Short-wave radiation received over a surface is a major determinant of both the local meteorology and the amount of melt that a snow or ice surface may undergo. However, when applying radiation models to raster surfaces we find that the grid resolution has a marked effect on the radiation load over a given area. For example, a radiation loading model applied to a 25m resolution digital elevation model (DEM) will not account for surface textures smaller than the actual pixel size. By applying a radiation loading model to a higher resolution DEM, we are able to account for such textural considerations as local shadowing, slope and aspect. In this study high resolution data has been obtained from an airborne scanning LASER altimetry survey of Peyto Glacier and the Wapta Icefields in the Canadian Rockies. The LASER altimetry data, surveyed by *Optech, Inc*., has been gridded to 2.5 m and 25 m resolutions for this comparative study. The purpose of this study is to compare the results of a short-wave radiation loading model of energy flux density (W m^{-2}) applied over a 25-metre DEM and a 2.5-metre DEM of Peyto Glacier in the Canadian Rocky Mountains. The results of this study illustrate that radiation load is primarily influenced by terrain slope, which reduces radiation load upon a surface by between 1 and 6 W m^{-2} as derived from the higher resolution DEM. Texture has also been examined using Landsat TM data of the study area.

INTRODUCTION

Radiation loading incident upon a surface is one of the controlling mechanisms on the local energy balance within a given area (Barry, 1992; Oke, 1996). Differences in elevation, surface aspect, slope and areas within shadow will alter the amount of radiation received on a given surface (Hay, 1977). Thus the temporal and spatial changes in the radiation load over a surface is a factor in both the energy and hydrological balance of that surface, thereby playing a significant role in the meteorology (McCutchan and Fox, 1986), soil temperature (Barry, 1992), snow melt regimes, etc. (Tabony, 1985; Barry, 1992) within localised and similar areas.

Although temperature is regularly used in many hydrological melt models, net radiation over a surface is known to be the more controlling influence on melt (e.g. Elder et al. 1998). Thus the surface data to be used in models must exhibit, with reasonable accuracy, higher resolution features in order to improve the modelling of physical processes at the surface. In many melt and hydrological modelling schemes, however, we are limited to fairly low resolution DEM's, such as the 7.5-minute (30m by 30m) DEM's produced by the United States Geological Survey, or 25m resolution Landsat TM imagery (for landcover classifications).

Studies that apply hydrological melt models tend to use spatial (DEM or other) data that are convenient, and may exclude some of the sub-pixel features that are equally as important. Often the spatial datasets that they use are inappropriately of too low a resolution for the study. High

[1] Waterloo Laboratory for Earth Observations, Department of Geography, University of Waterloo, Waterloo, ON N2L 1G3 CANADA, lechasme@yahoo.ca
[2] Cold Regions Research Centre, Wilfrid Laurier University, Waterloo, ON N2L 3C5 CANADA, chopkins@wlu.ca

resolution DEM's for a particular location are often i) difficult to find, and ii) are expensive to obtain from manual surveying. Thus topographic parameters may be only roughly approximated, but are nonetheless used when predicting the life of a glacier, hydrological cycles within complex terrain, and so on.

The purpose of this study is to explore the potential errors (over-estimations and under-estimations) in modelled radiation load when applied to a 2.5m DEM and a 25m DEM. Scaling issues are addressed within this paper to illustrate errors accrued when using lower resolution DEM's for general modelling purposes. The radiation model (Garnier and Ohmura, 1970; Barry, 1992; Oke, 1996) includes both direct and quasi-diffuse components, and has been used qualitatively to examine the radiation loading differences between a 25m resolution DEM and a 2.5m resolution DEM. Both DEM's have been derived from the airborne LASER altimetry data collected over Peyto Glacier, Canadian Rockies in October 2000. Collected radiation data and energy balance modelling over Peyto Glacier has been studied extensively by Munro (e.g. Munro, 1990). The objectives of this study include the following:

1. To examine changes in radiation loading between a 25m resolution DEM and a 2.5m resolution DEM for 12:00 on June 21st, and 8:00 on December 21st.
2. To investigate the controlling influences of surface texture resulting from different land covers, slopes and aspects.

STUDY AREA

The study area includes Peyto Glacier located at the headwater of the North Saskatchewan River Basin in the Canadian Rocky Mountains, Alberta (Figure 1). Peyto Glacier is one of many glaciers that feed out of the Wapta and Waputik Icefields and has been extensively studied since 1966. The life span of the glacier is of interest for future water resources prediction in Alberta. Elevation ranges from 2140m to 3180 m.a.s.l. and glacier area is approximately 12km^2. The surrounding topography is variable and is surrounded primarily by mountains and glacial moraines. The Wapta Icefield is fairly flat with few undulations, except in the crevasse fields located on the glacier.

AIRBORNE LIDAR DATA ACQUISITION AND PROCESSING

Peyto Glacier has been selected and subset from a larger LiDAR survey of the Wapta and Waputik Icefields commissioned by the National Glaciology Program of the Geological Survey of Canada, October 2000 (Demuth et al. *submitted;* Hopkinson, et al. 2001a) and flown by *Optech, Inc.* (Figure 1). This LiDAR survey is the first known survey using *Optech* Airborne Laser Mapping Technology (ALTM) over high elevation and varied terrain.

The purpose of a LiDAR (Light Detection and Ranging) or Laser altimetry survey is to determine the surface elevation or DEM along a proposed line of flight. In this study, an *Optech, Inc.* ALTM 1225 with a high pulse frequency of 25KHz at a wavelength of 1064nm was used. Airborne LASER altimetry is becoming an increasingly popular method of analysis in such areas as forestry (St-Onge et al. 2000; Hopkinson et al. *in press*), glaciology (Demuth et al. *submitted*), and shoreline mapping (e.g. Flood and Gutelius, 1997). ALTM (Airborne Laser Terrain Mapping) equipment combines the use of laser technology, the location of the laser head in space and time, and also temporal measurement of laser pulse transmission to reception in order to determine the horizontal and vertical coordinates of a point on the ground. The ALTM utilises scanning technology, whereby laser pulses are swept left and right perpendicular to the flight line, creating a "saw tooth" pattern of ground points. The resultant data can be used to create a high-resolution DEM of the ground surface using horizontal (x and y) and vertical (z) data collected by the scanning LASER. The vertical and horizontal accuracy of the collected ground points is dependent on referencing the LASER head to known control points on the ground. Referencing of ground points is achieved using differential GPS, whereby at least one GPS receiver and antenna is located over a known control point within 50 km of the survey area, and another is located inside the aircraft. Thus, through post processing of the aircraft GPS trajectory, the location of the LASER head is fixed in space every second. The quality of the final data product is largely related to the accuracy of the GPS trajectory. The normal accuracy for a LiDAR DEM tends to be within

20cms, and is therefore related to the GPS trajectory and not the LASER-head. Further refinement of the trajectory and compensation for aircraft attitude variation (pitch, roll and yaw) is achieved by post processing data collected by an onboard inertial navigation system (INS) at 50 Hz. Current technology can collect multiple returns at a pulse repetition frequency (PRF) greater than 33 KHz. Laser spot spacing on the ground can be as low as 50cm in both the x and y directions. The ground swath typically varies between zero and 2000m depending on flying altitude and scan angle.

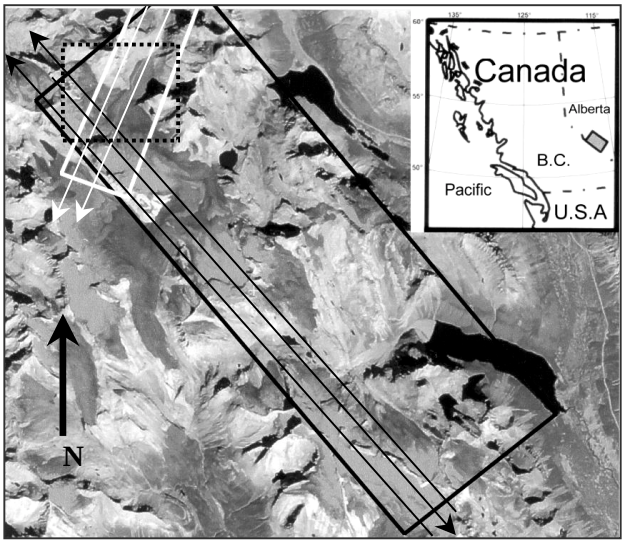

Figure 1: Study area and flight polygons over the Continental Divide and Peyto Glacier. The first polygon is illustrated in black with arrows representing the flight paths taken during the survey. The second polygon is shown in white, with similar flight lines. The dashed box represents the location of the study area. Inset: the location of the survey within Alberta, Canada.

Two flight polygons (Figure 1) planned for the study consisted of: 1) a SE - NW survey polygon along the Continental Divide (outlined in black) and 2) a smaller SSW-NNE survey polygon along the Peyto Glacier axis (outlined in white). Table 1 displays the flight and sensor parameters used during the airborne LiDAR survey of the study area. Also shown are the raw output specifications, which illustrate that ground survey point spacing varied between one and three metres, depending on surface elevation. For a comprehensive description of data acquisition, the reader is referred to Demuth et al. (*submitted*) and Hopkinson, (2001a).

Table 1: Survey input and output parameters used during the airborne LiDAR survey

Input		Output	Height in metres above ground level		
Laser and Flight Settings		Parameter	900	1600	2300
Repetition Rate	25 kHz	X spacing	1.40	1.40	1.40
Scanner Frequency	20 Hz	Y spacing	1.05	1.86	2.68
Scan Angle	+/-20^o	Footprint	0.24	0.41	0.59
Aircraft Velocity	55 m/s	Swath width	655	1165	1674
Flying Altitude	~4000m				
Max. Bank Angle	20^o				
Line Spacing	500m				

For this analysis we have gridded the LiDAR data into two separate resolutions in a DEM analysis package called 'Surfer'. The first dataset consists of a 25m raster DEM, typical of Landsat imagery and of a slightly higher resolution than 7.5 second USGS DEMs (Figure 2 a). The second dataset consists of a high resolution 2.5m DEM (Figure 2 b). In the 2.5m DEM we are able to define numerous surface features that are either partially visible or not visible in the lower resolution 25m DEM. These include crevasses, moulins, melt streams, and variations in topography in the mountains surrounding the glacier (Figure 2).

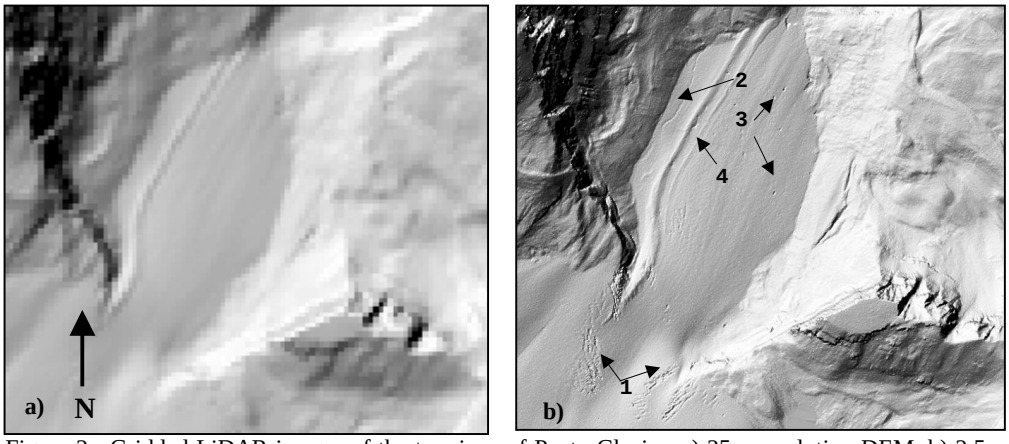

Figure 2: Gridded LiDAR images of the terminus of Peyto Glacier; a) 25m resolution DEM, b) 2.5m resolution DEM. Notice the detail and location of 1) crevasse fields, 2) a surface melt stream, 3) moulins, and 4) the medial moraine in the 2.5m image.

RADIATION MODELLING IN ARC/INFO

The shortwave radiation algorithm that was used for this study was first proposed by Garnier and Ohmura in 1968, and has since become an accepted basis for many of the radiation models used today (Dozier, 1980; Barry, 1992, Elder et al. 1998). The radiation model combines diurnal solar geometries as they change throughout a given year with slope orientation geometries (refer to Oke, 1996) calculated from the gridded LiDAR DEM in ArcINFO. For this study, we have chosen June 21st and December 21st solstices at 12:00 pm and 8:00 am, respectively, thus illustrating the maximum extent of modelled shortwave radiation received within the glacierised basin. Figure 3 illustrates the model routines used within the analysis for both the 2.5m and the 25m gridded LiDAR data.

Surface and solar geometries were easily related to derive incoming shortwave radiation loading incident upon a surface during a clear sky (Figure 3). However the shortwave radiation model proposed initially by Garnier and Ohmura (1968) does not account for the effects of shadowing, skyview of individual pixels, or the diffuse component. Obstacle shadowing has been derived using the shadowing function in ArcINFO:

1. Shadows have been calculated from the original LiDAR DEM by specifying an imaginary solar path length, which includes solar azimuth and altitude at a specific time on a certain day (in this case, either 12:00pm, June 21st or 8:00am, December 21st).
2. A binary raster grid of shadow and non-shadow areas has been computed, assigning areas that are not in shadow, a value of one.
3. The shadow map was then multiplied with the resulting direct beam radiation map, whereby areas that are not in shadow retain the modelled direct beam and areas that are in shadow receive a value of zero.

Skyview provides a percentage of viewable sky for each pixel and is important for calculations of diffuse radiation because sky obstructions will have an influence on the amount of diffuse radiation received. Numerous radiation models employ the use of a skyview or 'viewshed' function (i.e. Dozier and Frew 1990) An empirical sky view calculation is applied to each pixel within the original LiDAR DEM. The skyview is calculated such that

$$Skyview = \left(\frac{LiDAR\ DEM}{2900}\right) \times \left(\left(\frac{90^{O} - Slope}{180^{O}}\right) + 0.5\right) \qquad [1]$$

where '2900' is approximately the elevation in metres at the top of the icefield and 'slope' is the slope (degrees) map created from the original DEM. Therefore elevations above 2900m that are on flat surfaces will likely receive greater than 100 percent of the diffuse sky radiation due to terrain

irradiance. Elevations below 2900m must have a skyview of less than one due to surrounding mountains. As slope increases, the skyview decreases to a minimum slope value of 0.5 (Table 2).

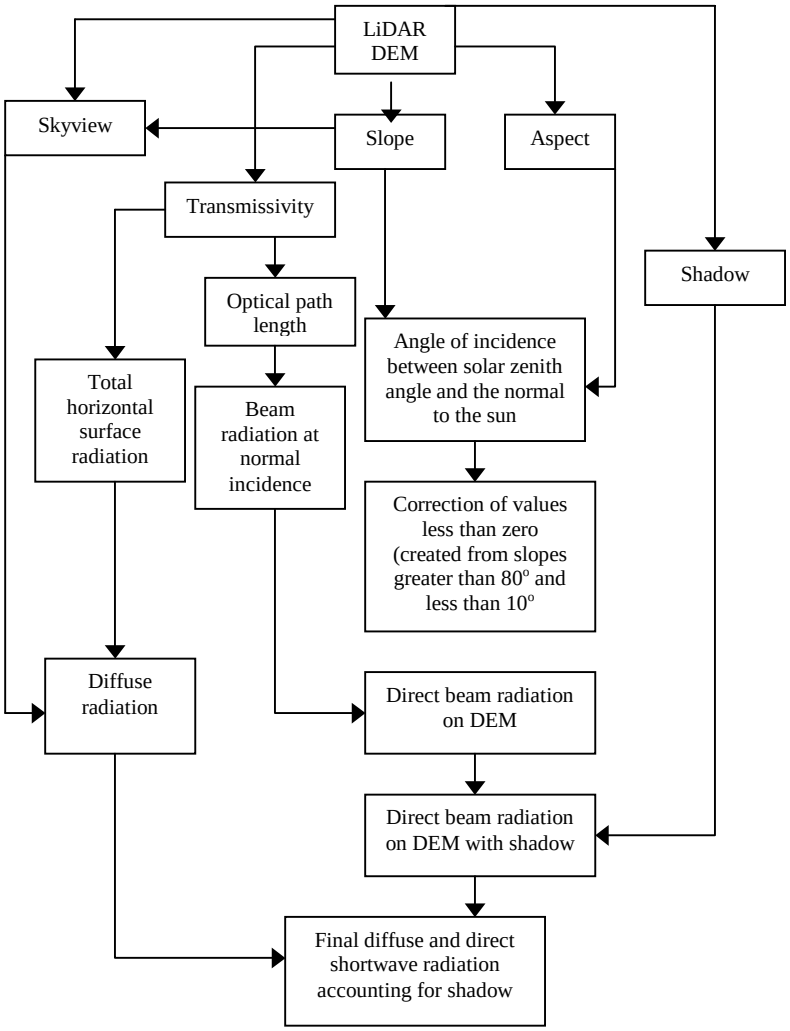

Figure 3: Flow diagram of the shortwave radiation model used for the analysis. Boxes represent surface measurement coverages calculated in ArcINFO.

Table 2: Examples of sky view based on slope and elevation

	Slope		
Elevation (m)	*0°*	*45°*	*90°*
2000	69%	52%	35%
3300	114%	86%	57%

The diffuse radiation component has been empirically calculated such that diffuse radiation is an estimated 10 percent of the total horizontal surface radiation. The amount of diffuse radiation during clear sky conditions depends on altitude, season, and atmospheric conditions and can vary between eight and 15 percent of horizontal surface radiation (Barry, 1992). Therefore an average seasonal and altitudinal diffuse radiation component of 10 percent has been used. Variations in the overall direct and diffuse shortwave radiation loading calculated by this simplistic empirical model are approximations to illustrate differences between the two DEMs used.

Finally, a Landsat TM image of the study area taken on September 7th 1998 has been included in the analysis to aid in the characterisation of textures and influence on direct solar radiation

(shadowing and direct receipt). The Landsat TM image has been classified into four land classes using a maximum likelihood supervised classification (Lillesand and Kieffer, 1994). Similarly both slope and aspect derived DEMs have been reclassified into four discrete classes for comparison (discussed later in the text). Textural analysis has been performed using a windowed standard deviation neighbourhood operation on the radiation loading images at 25m and 2.5m. Through the neighbourhood operation, we were able to investigate the relationship between texture and radiation variability within the images and also, the greatest influence on radiation variability (slope, aspect, or land cover type).

RESULTS AND DISCUSSION

Radiation Loading Model

The radiation model illustrated in Figure 3 has been applied to both the 25m and the 2.5m DEMs of Peyto Glacier. Modelled radiation flux density ranges from 33 to 1168 Wm^{-2} for a cloudless day on June 21st at 12:00pm (Figure 4) illustrated for both the 25m and 2.5m images. The range of radiation flux density for the winter (December 21st, 8:00am) image is between 3 Wm^{-2} in shadow areas to 145 Wm^{-2} for slopes facing solar azimuth (Figure 5). Radiation loads predicted using the model have not been validated with field data, but are considered adequate for the purpose of investigating scaling issues. Table 3 summarises the influence of terrain slope and aspect on modelled radiation loading.

Table 3: General radiation flux density (W m^{-2}) received on varying slope orientations and angles (without shadows)

	Slope Angle							
	Winter (December 21) 8:00am				*Summer (June 21) 12:00pm*			
Slope Orientation	0^o	30^o	60^o	90^o	0^o	30^o	60^o	90^o
North	7-25	5-25	4-25	3-25	778-930	406-574	43-218	33-218
South	55-69	69-84	4-25	3-25	930-1040	930-1040	812-930	693-812
East	69-84	99-114	99-129	119-129	930-1040	812-930	693-812	574-693
West	10-25	10-25	10-25	10-25	930-1040	574-693	574-693	693-812

Typically, east-facing slopes tend to receive the greatest amount of radiation at 8:00am on December 21st. Surfaces with a slope of zero degrees and a south-east aspect tend to receive the greatest amount of radiation at 12:00pm on June 21st. The importance of terrain aspect and azimuth on solar radiation are illustrated for crevasses and highly variable bare rock surfaces in Figure 4 (magnified images). Notice both the shadowing and direct radiation components found over both types of surfaces (crevasses and bare rock). Thus radiation loading patterns over crevasse fields for both resolutions are markedly different, with the 25m model displaying a homogenous radiation load in this area. Similar observations can also be made for the December 21st radiation loading images (Figure 5). Although radiation flux density is visibly homogenised at the 25m resolution, it needs to be ascertained as to the type of features located at sub-pixel level and whether or not these will have markedly different radiation load in shadow and non-shadow areas.

Radiation (Wm^{-2}) averages for the 25m and 2.5m images are shown in Table 4 for both summer and winter. During the summer, slightly greater extremes are found in the 2.5m images over the 25m images. A greater range in radiation flux density in the 2.5m radiation images is to be expected as the increased resolution will create localised highs and lows in radiation load that are smoothed over in the lower resolution images (Figures 4 and 5). The mean radiation flux density is lower on both 2.5m images, due to the effects of shadows not observed in the 25m images. In order to observe the differences in radiation loading between the 25m resolution images and the 2.5m resolution images, the 25m resolution radiation loading images have been resampled to 2.5m and subtracted from the original 2.5m images for summer radiation loading (Figure 6). Differences in winter radiation loading have not been illustrated, but the observations are similar to those of the summer radiation differences. Statistical information is presented in Table 4 where

positive difference values indicate higher radiation flux density derived for the 25m DEM and negative values indicate higher radiation flux density derived for the 2.5m DEM.

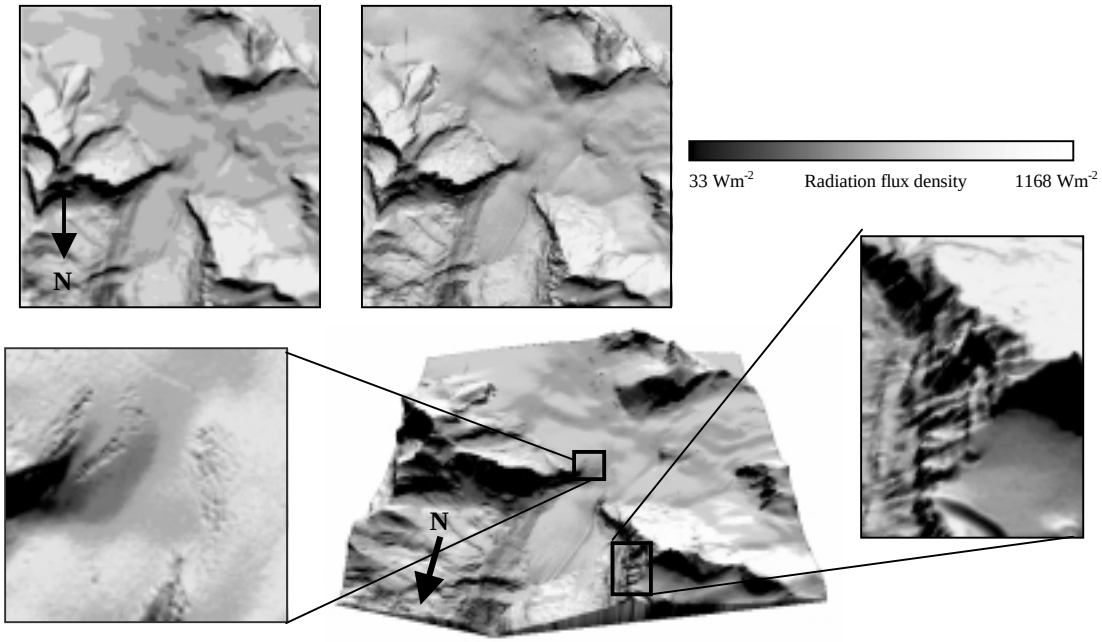

Figure 4: Radiation loading incident upon Peyto Glacier at 25m and 2.5m resolution for June 21st. Also illustrated is a 3D terrain at 2.5m resolution of the radiation loading images. Shadowing/illumination of various features has been highlighted in magnified images. Note orientation of images (orientation has been changed to illustrate shadowed areas).

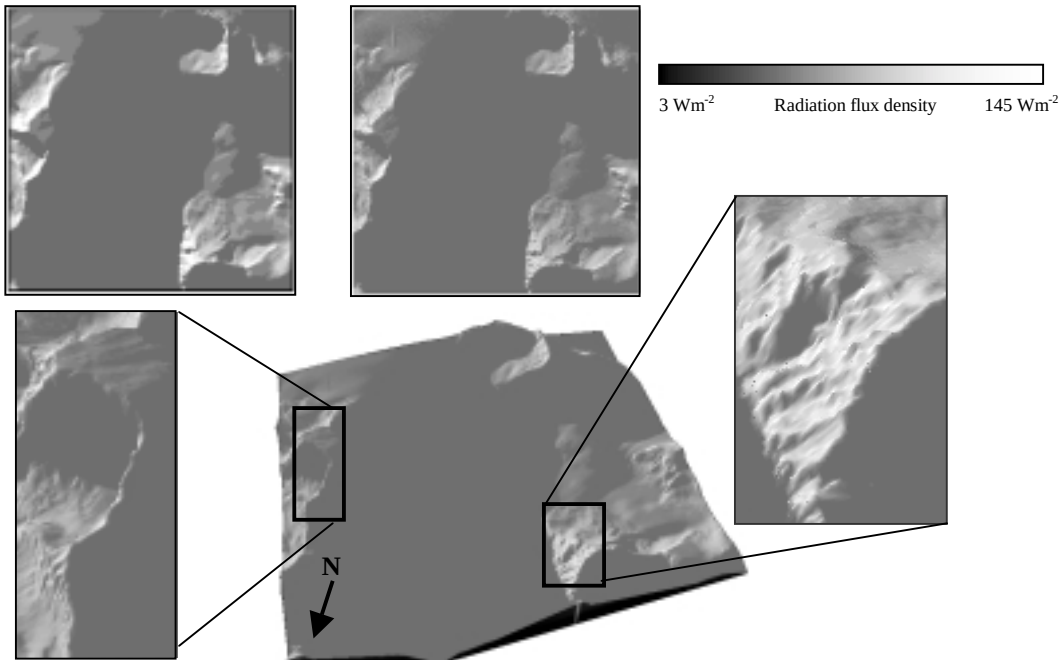

Figure 5: Radiation loading incident upon Peyto Glacier at 25m and 2.5m resolution for December 21st. Similar to Figure 4, a 3D terrain model is also shown for the 2.5m resolution radiation loading results. Again, areas of high texture and shadowing are illustrated.

Table 4. Statistics for the 2.5m and 25m summer and winter radiationflux density (Wm^{-2}) and differences between 2.5m and 25m radiation loading for summer and winter (resampled to 2.5m).

Summer Statistics	2.5m Image	25m Image	Difference	Winter Statistics	2.5m Image	25m Image	Difference
Minimum	33	33	0	Minimum	3	3	0
Maximum	1168	1166	-2	Maximum	144	127	-17
Mean	908	914	6	Mean	20	21	1
Standard Deviation	189	178	-11	Standard Deviation	19	18	-1

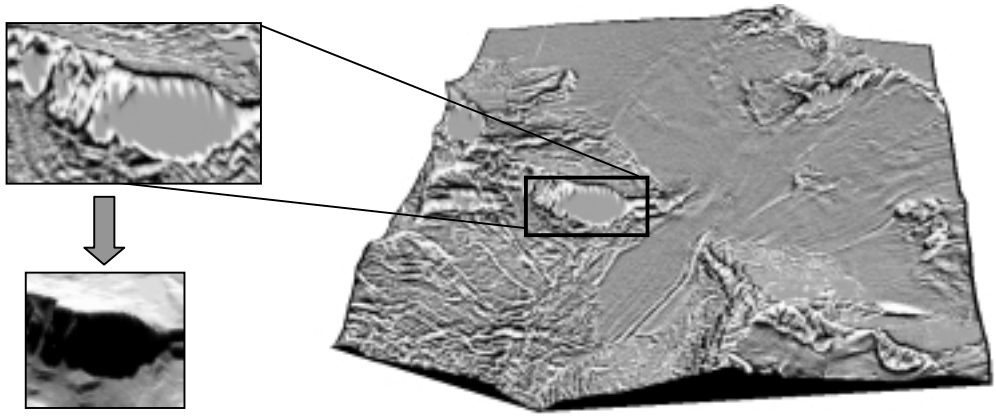

Figure 6: Difference in radiation flux between the 25m resolution image and the 2.5m resolution image for 12:00pm, June 21st. White areas indicate where radiation is calculated higher for the 25m image, and black areas illustrate higher radiation loading calculated for the 2.5m image. Grey represents minimal difference between the images. Inset images illustrate the difference in radiation loading for a shadowed area and the original radiation loading DEM facing NNW from Mount Thompson. Notice white areas within the shadowed region in the inset image. These differences are created due to the generalised higher radiation loading of the 25m DEM and the definition of shadowed areas in the 2.5m DEM. Therefore these white areas of over-estimation are actually outlines of shadowed areas derived from the 2.5m DEM.

Differences in radiation load tend to be most evident in shadowed areas and along the tops of ridges and gullies. Further, radiation variability is 10% greater within the 2.5m DEM. The following observations are made:

1. Resolution has a greater effect at low incident angles due to long shadows. For example, high resolution textures will exhibit shadows that may be missed in a lower resolution image.
2. Radiation load is overestimated on the tops of gullies, and is often underestimated near the bottom of gullies in the 25m DEM (Figures 4 to 7).
3. Solar radiation is often underestimated on the sides of ridges that are facing the sun, and are overestimated on the shadow side of slopes. These are caused by mixed pixels, which ignore areas of shadowing versus areas exposed to sunlight in generally shadowed areas (magnified image in Figure 6).
4. A general overestimation in solar radiation loading exists over the entire 25m DEM. These differences will alter as both days and hours change.
5. The minimum calculated radiation flux density is the same for both images, as to be expected.
6. The maximum radiation load is greater on the 2.5m DEM than on the 25m DEM for both summer and winter. The higher resolution DEM increases the probability of a pixel being angled normal to the solar beam. This is more prevalent in winter when the 2.5m model has a maximum radiation load of 17 Wm^{-2} greater than that derived for the 25m DEM.

Texture Analysis

In the last section, we have shown that shadowing and illumination are directly influenced by the variability of the terrain evident in the 2.5m resolution DEM. Further, the 25m resolution DEM is unable to accurately discriminate between smaller, yet significant features in the

landscape. Terrain slope, azimuth, and land cover each influence the variability of the terrain, yet it is difficult to determine which has the greatest influence on radiation properties at the surface. Variability in radiation loading was considered using a roaming window technique to examine the standard deviation within a 250m by 250m box. The roaming window technique is used as a filter to find the summary standard deviation within a 10 by 10 pixel area (or 100 by 100 pixel area in the 2.5m DEM). Therefore areas of higher standard deviation are representative of high radiation variability and therefore, higher textured areas within the image. Figure 7 a) illustrates the results of the neighbourhood operation on the 25m resolution radiation flux density DEM, where darker regions represent areas of greater radiation variability. The same analysis has been performed on the 2.5m image (not shown). Differences between the 25m DEM and the 2.5m DEM are illustrated in Figure 7 b). Figure 7 more quantitatively illustrates the relationship between texture and radiation load, as discussed in the last section.

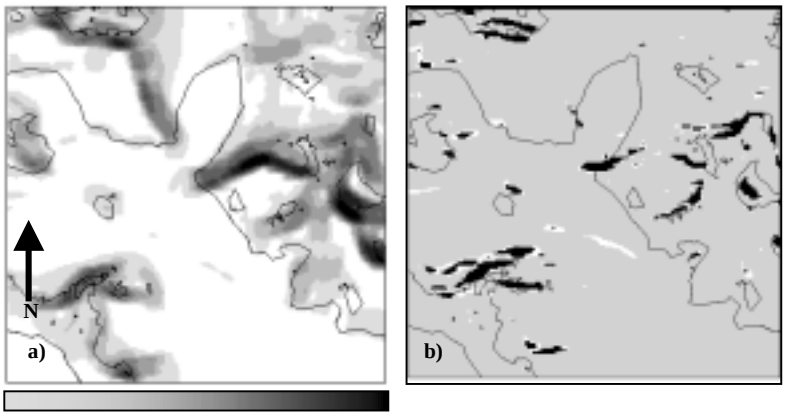

Figure 7: Analysis of variability in the summer 25m resolution image a) is determined using a neighbourhood operation of standard deviation within the radiation flux density image (Figure 4). Greatest variability in solar radiation loading is shown in black and dark grey. Lower variabilities in radiation loading can be found on flatter surfaces (light grey to white). b) the difference in calculated radiation loading variability between the 25m and 2.5m DEMs. Black areas occur where the 25m radiation image has higher variability, while grey areas indicate where the 2.5m radiation image has higher variability. White shows areas of little difference.

Variations in radiation load are generally low on the glacier, except on crevasse fields, where shadowing and direct illumination of crevasse sides is evident. Examination of Figure 7 b), illustrates that variations in radiation loading are generally greater for the 2.5m DEM. Interestingly, greater variations in the 25m image are prevalent in some areas. These include on the edges of major terrain shadows, where highly shadowed areas are within close proximity (within a neighbourhood of 10 by 10 pixels) of areas receiving direct solar radiation. This indicates that the more gradual variations in radiation variability found in the 2.5m radiation loading derived image are likely to be overlooked within the lower resolution 25m radiation image.

Slope and aspect models were computed and broken down into 4 equal groups, and the Landsat TM image classified into water, glacier, grass, and bare ground, respectively (Figure 8). Each of these terrain type parameters was compared with the derived radiation variability image. The mean of the standard deviation in radiation variability within each of the terrain types was calculated and is illustrated in Figure 8 for slope, aspect, and land cover terrain types for both the 25m and 2.5m resolution radiation loading images. Observations of higher radiation variability associated with texture in the 2.5m DEM is evident, with a marked increase in radiation variation found at slope angles of 68 to 90 degrees within the 25m DEM. Interestingly, surface slope tends to have the greatest influence on radiation variability, with standard deviations in radiation loading ranging from approximately 50 Wm^{-2} on fairly flat surfaces to approximately 340 Wm^{-2} on almost vertical slopes. As slope increases, influences of direct illumination and shadowing become more

prevalent, thereby increasing the range of radiation loading on these surfaces. Land surface type also plays a large role in shadowing, as more textured land surfaces will also increase the amount of shadows and directly illuminated pixels. Landcovers have been classified into four distinct categories. We will assume that areas classified as water will remain absolutely flat with a 0^o slope and no aspect. Glacial surfaces are slightly more variable, as are grass areas, both of which contain undulating topographies. Finally, bare ground represents many of the mountainous areas found within this particular image. Thus areas of bare ground are often associated with a highly varying topography within the Peyto Glacier basin but cannot always be assumed to be highly variable (i.e. the surface may also be flat and moderately smooth). As illustrated in Figure 4, a significant portion of the study area contains topographically variable bare ground with large slope angles. As such, bare ground in this area is associated with significant variations in radiation loading. However, its influence is much less than that of slope alone.

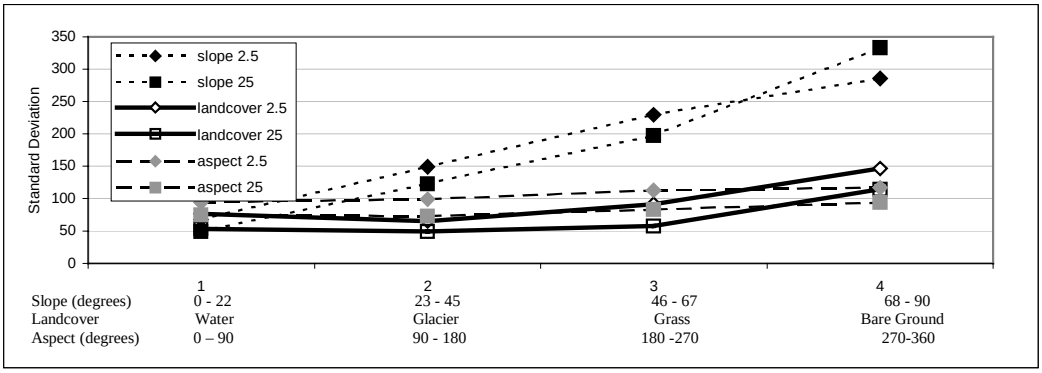

Figure 8: The influence of changing slope, land cover, and aspect on radiation variability on the Peyto Glacier LiDAR DEM for June 21st at 12:00pm.

CONCLUSION

In this study we have used two gridded LiDAR DEM's of 25m and 2.5m obtained from a LiDAR survey of Peyto Glacier basin to determine the effects of scale on radiation flux density derived from a simple radiation loading model. The acquisition of a high resolution DEM for the purposes of radiation modelling has improved our ability to examine radiation load patterns on surfaces that may otherwise be ignored or 'smoothed over' in a lower resolution DEM. The following objectives have been met:

1. Changes in radiation loading between a 25m resolution DEM and a 2.5m resolution DEM for 12:00 on June 21st, and 8:00 on December 21st have been studied.

Radiation loading tends to be overestimated on the lower resolution 25m DEM for both summer and winter derived radiation flux density (Wm^{-2}). During times of low sun angle and low shadows, the 25m model overestimates mean radiation by five percent (1 Wm^{-2}) over the entire DEM. Yet maximum radiation load is under estimated by 13% (17 Wm^{-2}). The same pattern is evident for high sun angles, but the magnitude is significantly reduced.

2. Surface texture and influence on radiation has been investigated by examining different land covers, slopes and aspects.

Regions of greatest radiation variability tend to occur on surfaces that are most highly textured, for example, bare ground. Although land cover and aspect play an important role in the overall radiation load on a surface, we have found that terrain slope has the most influence on variations in radiation load. However, areas of large slope angles are often also bare ground and of varying aspects. Therefore slope may not always play such a large role in the variability of radiation load in other DEMs with different landcovers. In general, glacial areas tend to have fairly low variability in radiation load, except in areas that are prone to crevasses and moulins (especially along the sides of these features). In these regions, we find that the radiation load varies considerably from the 25m DEM to the 2.5m DEM, where shadowing and direct illumination is evident. Thus it is within these areas of high variability that hydrological and melt models must be particularly accurate, especially when glacial mass balance is concerned.

In summary, it has been demonstrated that low resolution DEMs can lead to a systematic overestimation of mean radiation load and a systematic underestimation of peak radiation load over a ground surface. These results may have significant implications for those utilising low resolution radiation loading models for hydrological, energy balance, and meteorological studies. For example, systematic scale induced radiation load biases over a snow covered or glacierised surface may introduce error in hydrological yield calculation using a radiation melt model. The next stage of this analysis is to generate a model of radiation loading 'uncertainty' or 'potential for systematic bias' based upon terrain and land cover types.

ACKNOWLEDGEMENTS

The authors would like to thank Mike Demuth at the National Glaciology Program, Geological Survey of Canada for giving us permission to use the LiDAR dataset, *Optech Inc.* for flying the survey, and Mike Sitar (*Optech Inc.* and the Cold Regions Research Centre, Wilfrid Laurier University) for assisting with raw data generation. Partial funding was provided by an NSERC graduate student scholarship.

REFERENCES

Barry, R. G., 1992: *Mountain Weather and Climate, 2nd ed.* New York: Routledge. 402 pgs.

Demuth, M., C. Hopkinson, M. Sitar, A. Pietroniro, and L. Chasmer: Airborne scanning LASER terrain mapping of Peyto Glacier, Wapta and Waputik Icefields, Canada: First results and future prospects. *Submitted to Annals of Glaciology.*

Dozier, J., 1980: A clear-sky spectral solar radiation model for snow-covered mountainous terrain. *Water Resources Research,* 16:709-718.

Dozier, J. and J. Frew, 1990: Rapid calculation of terrain parameters for radiation modeling from digital elevation model data. *IEEE Transactions on Geoscience and Remote Sensing*, 28:963-969.

Elder, K., W. Rosenthal, and R. Davis, 1998: Estimating the spatial distribution of snow water equivalence in a montane watershed. *Hydrological Processes*, 12:1793-1808.

Flood, M., and B. Gutelius, 1997. Commercial implications of topographic terrain mapping using scanning airborne laser radar. *Photogrammetric Engineering and Remote Sensing.* 63(4):327-366.

Garnier, B. J., and A. Ohmura, 1970: The evaluation of surface variations in solar radiation income. *Solar energy*, 13:21-34.

Hay, J. E., 1977: An analysis of solar radiation data for selected locations in Canada.*Climatological Studies*, 32. Atmospheric Environment Service, Downsview, Ontario.

Hopkinson, C., M. Demuth, M. Sitar, and L. Chasmer, 2001: Applications of LiDAR mapping in a glacierised mountainous terrain. *Proceedings of the International Geoscience and Remote Sensing Symposium*, Sydney, Australia. July 9 – 14.

Hopkinson, C., and others, *in press*: Mapping the spatial distribution of snowpack depth beneath a variable forest canopy using airborne laser altimetry. *Proceedings of the Eastern Snow Conference*, Ottawa, May 14-18, 2001.

Lillesand, T. M., and R. W. Kiefer: *Remote Sensing and Image Interpretation* 3rd Ed. Toronto, John Wiley and Sons, Inc. 1994. pp. 750.

McCutchan, M. H., and D. G. Fox, 1986: Effect of elevation and aspect on wind, temperature and humidity. *Journal of Climatology and Applied Meteorology*, 25:1996-2013.

Means, J., S. Acker, B. Fitt, M. Renslow, L. Emerson, and C. Hendrix, 2000: Predicting forest stand characteristics with airborne scanning LiDAR. *Photogrammetric Engineering and Remote Sensing.* 66(11):1367-1371.

Munro, D. S. 1990: Comparison of melt energy computations and ablatometer measurements on modelling ice and snow. *Arctic and Alpine Research.* 22(2):153-162.

St-Onge, B., J. Dufort, and R. Lepage, 2000: Measuring tree height using scanning laser altimetry. Proceedings of the 22nd Annual Canadian Remote Sensing Symposium, Victoria, British Columbia, Canada. August 21 – 25, 2000.

Ohmura, A., 1968: The computation of direct insolation on a slope. *Climatological Bulletin*, 3:42 -53.

Oke, T.R., 1996: Boundary Layer Climates. London: Routledge, International Thomson Publishing Company, 435 pp.

Tabony, R. C., 1985: Relations between minimum temperature and topography in Great Britain, Journal of Climatology 5:503-520.